PACIFIC EARTHQUAKE ENGINEERING RESEARCH CENTER

A Granular Framework for Modeling the Capacity Loss and Recovery of Regional Transportation Networks under Seismic Hazards: A Case Study on the Port of Los Angeles

Michael Benedict Virtucio[1]
Barbaros Cetiner[2]
Bingyu Zhao[1,3]
Kenichi Soga[1]
Ertugrul Taciroglu[4]

[1]Department of Civil and Environmental Engineering
University of California, Berkeley, USA
[2]NHERI SimCenter
University of California, Berkeley, USA

[3]TU Wien, Austria

[4]Department of Civil and Environmental Engineering
University of California, Los Angeles, USA

A Granular Framework for Modeling the Capacity Loss and Recovery of Regional Transportation Networks under Seismic Hazards: A Case Study on the Port of Los Angeles

Michael Benedict Virtucio[1]

Barbaros Cetiner[2]

Bingyu Zhao[1,3]

Kenichi Soga[1]

Ertugrul Taciroglu[4]

[1]Department of Civil and Environmental Engineering
University of California, Berkeley, USA
[2]NHERI SimCenter
University of California, Berkeley, USA
[3]TU Wien, Austria
[4]Department of Civil and Environmental Engineering
University of California, Los Angeles, USA

ABSTRACT

Earthquakes, being both unpredictable and potentially destructive, pose great risks to critical infrastructure systems like transportation. It becomes crucial, therefore, to have both a fine-grained and holistic understanding of how the current state of a transportation system would fare during hypothetical hazard scenarios. This paper introduces a synthesis approach to assessing the impacts of earthquakes by coupling an image-based structure-and-site-specific bridge fragility generation methodology with regional-scale traffic simulations and economic loss prediction models. The proposed approach's use of context-rich data such as OpenStreetMap and Google Street View enables incorporating information that is abstracted in standard loss analysis tools like HAZUS in order to construct nonlinear bridge models and corresponding fragility functions. The framework uses a semi-dynamic traffic assignment model run on a regional traffic network that includes all freeways and local roads (1,444,790 edges) and outputs traffic volume on roads before and after bridge closures due to an earthquake as well as impacts to individual trips (42,056,426 trips). The combination of these models enables granularity, facilitating a bottom-up approach to estimating costs incurred solely due to physical damage to the transportation network. As a case study, the proposed framework is applied to the road network surrounding the Port of Los Angeles---an infrastructure of crucial importance---for assessing resilience and losses at a high resolution. It is found that the port area is disproportionately impacted in the hypothetical earthquake scenario, and delays in bridge repair can lead to a 50% increase in costs.

Keywords: Earthquake, recovery, economic, infrastructure, resilience, transportation, bridge

ACKNOWLEDGMENTS AND DISCLAIMER

CONTENTS

LIST OF TABLES

x

LIST OF FIGURES

1   INTRODUCTION

Natural hazards pose a significant risk to an area's critical infrastructure, and different areas may be more prone to certain hazards than others. For example, places like California are more prone to earthquakes and wildfires due to their geographic location, while states in the US Southeast and Midwest are more prone to hurricanes and flooding. Some hazards are easier to forecast and, consequentially, to prepare for, while others are more unpredictable and, therefore, can cause more damage and losses. Earthquakes are a good example of the latter. FEMA estimates that the US incurs a minimum Annual Earthquake Loss (AEL) of $6.1 billion per year, not yet including losses due to damage to lifeline infrastructure and indirect economic losses, 61% of which ($3.7 billion) is concentrated in California (Jaiswal et al., 2017). The report further indicates that 55 metropolitan areas account for 85% of this AEL, with Los Angeles accounting for 22% of it ($1.35 billion). With urbanization continuing to concentrate population and infrastructure in cities, areas with high seismic hazard and high building exposure—such as the Los Angeles and San Francisco Bay—rank high on AEL at over $100 per capita (Jaiswal et al., 2017).

The US Cybersecurity and Infrastructure Security Agency (CISA) defines critical infrastructure sectors as systems that are key to society's daily operations and any impairment, disruption, or destruction of which can have significant to devastating impacts on physical or economic security, public health, or safety[1]. Transportation infrastructure is an example of this. Transportation systems provide mobility to people, goods, and services that are vital to society's daily operations, which makes them even more important in times of crisis (Mattson and Jenelius, 2015) for scenarios like evacuation and emergency response. These infrastructure systems are built based on standards established at the time of construction that ensure a level of quality for a set amount of time. However, the average age of bridges in the US is 43 years old, very close to the typical 50-year design life (ASCE, 2021), and the American Society of Civil Engineers (ASCE) estimates that $123 billion (2017 values) are needed to rehabilitate all US bridges. With this context, discussions on transportation systems' vulnerability and resilience become crucial.

Resilience and vulnerability have been defined across different disciplines. Here, we interpret the former to mean the capacity of a system to retain functionality after experiencing an extreme event and to recover quickly from it. Goldberg (1975) defined resilience in socioecological systems as "the size of the perturbation that the system can withstand and still retain its essential characteristics". This definition transfers well into civil systems as Berdica (2002)'s landmark study more than a decade ago, prior to the establishment of resilience as a key term in engineering,

---

[1] US Cybersecurity & Infrastructure Security Agency, 2022. Infrastructure security. https://www.cisa.gov/infrastructure-security.

closely defines reliability in road transportation systems as the complement of vulnerability, defined as ``a susceptibility to incidents that can result in considerable reductions in road network serviceability''. Reductions in road network serviceability is the most direct impact of a lack of resilience in the transportation infrastructure; however, this can have further reaching implications than just a longer travel time. As defined by CISA, damage to critical infrastructure can impact economic security. Disruptions to the transport network's connectivity can result in economic losses for a variety of sectors (Cho et al., 2001). Given the unpredictability and potentially devastating impacts of a large earthquake in certain areas, it is important to adopt a holistic definition of resilience that encompasses direct and indirect impacts of seismic hazards to the transportation network and to the economy at large.

The next chapter lists the objectives of the study based on identified gaps to be addressed, provides the observations from a literature review conducted for this purpose and describes the organization of the report.

2   LITERATURE REVIEW

2.1   BRIDGE MODELING FOR PREDICTING SEISMIC DAMAGE

Assessing the seismic vulnerability of bridges consists of two main tasks. The first is the hazard characterization (e.g., the magnitude and epicenter of an earthquake, as well as the intensity or ground motion that characterize the severity of the probabilistic hazard at a location). McGuire (2001) identifies two different approaches: deterministic versus probabilistic, and also identifies which approach is appropriate to use based on the ultimate decision trying to be made. The second task is the development of models or relationships that establish a connection between the hazard characteristics (e.g., an earthquake intensity measure) and the severity of bridge damage. Previous work on resilience assessment has used different approaches in modeling the effects of seismic hazards on bridges. Some focus on analyzing past earthquake scenarios and therefore use collected historical data of bridge damage to aid in quantifying costs and resilience (Chang and Nojima, 2001). For those more concerned with predicting the effects of future or hypothetical scenarios, a popular way to model bridges' behavior under seismic hazards is through the use of fragility curves that take into account different types of bridge material and composition and their historical behavior under earthquake scenarios (Nojima and Sugito, 2000). HAZUS developed by FEMA has a database, including those from the National Bridge Inventory (NBI), of such curves that have been used extensively by prior studies (Frangopol and Bocchini, 2011). NBI has a comprehensive database of bridges, including information like year built, year reconstructed, material type, functional classifications, etc. Works like Padgett et al. (2010), which sought to model 375 bridges for South Carolina, simplified classifications using two characteristics: span configuration and girder material type, leading to 11 bridge types. However, a common method employed by some studies is to assume that bridges in an area have the same structural type, mostly modeled as multi-span simply supported (MSSS) reinforced concrete or steel bridges to simplify bridge modeling and analysis (Nielson, 2005; Feng et al., 2020; Chang et al., 2012). Recently, new data sources have been explored to inform the development of more detailed and granular structural models for bridges: Google Street View and satellite images are just a few of these new data sources that are also openly available. Their use cases have been demonstrated[2] in Cetiner (2022) where highly accurate models for individual bridges are constructed in a semi-automated image-based process.

---

[2] Cetiner, B., Wang, C., McKenna, F., Hornauer, S., Guo, Y., Yu, S., Taciroglu, E., Law, K., 2022. Nheri-simcenter/brails: Release v3.0.0. URL: https://zenodo.org/record/7132010, doi:10.5281/zenodo.7132010.

2.2 TRAFFIC MODELING UNDER EARTHQUAKE SCENARIOS

Similar to the bridge vulnerability research, some previous traffic modeling work focuses on analyzing past earthquake scenarios and used collected historical data of transportation network performance to understand resilience (Chang and Nojima, 2001). Others like Frangopol and Bocchini (2011) focused more on bridge rehabilitation strategies, with the aim to minimize cost and maximize resilience. But many of such studies use transportation network characteristics such as capacity and connectivity to generate a priority list without considering the changing traffic flow characteristics after a natural hazard using traffic simulations.

For those that focus on future and hypothetical scenarios, however, using traffic simulation models is a popular approach, which generally includes two categories. The first one is macroscopic modeling, wherein the traffic flow is represented in terms of aggregate measures like flow, space-mean speed, and traffic density. Payne (1979) states that these models sacrifice detail for efficiency and the ability to analyze problems of much larger scope. Microscopic models, on the other hand, are on the level of the individual movement of vehicles (Payne, 1979). The main drawback of microscopic models is the high computational demands required to run simulation models, especially for large networks. Wu et al. (2021) utilized microscopic models to simulate traffic flows of a very small transportation network with only around 30 links and 20 nodes.

Some studies have tried to find the middle ground between macroscopic and microscopic models to find a good balance between granularity and simplicity. Static traffic models, which include the all-or-nothing method, is the most basic form of trip assignment as it assumes no congestion and that all traffic simply chooses their respective shortest paths (Modarres and Zarei, 2002; Nakanishi et al., 2013; Cho et al., 2001). This allows for the analysis of slightly larger networks with Modarres and Zarei (2002) analyzing 534 links and Cho et al. (2001) analyzing as many as 20,000 links. Alipour and Shafei (2016) used static traffic assignment but operated on the traffic analysis zone (TAZ) level with 1,527 TAZs representing Los Angeles and Orange Counties—an approach that sacrifices a considerable amount of resolution as each TAZ covers 4 square miles on average. Zhou et al. (2010) used traffic assignment on the node level but condensed the origin-destination (OD) pairs to only 148 representative nodes in the network.

Contrary to static assignment models, dynamic traffic assignment models have a notion of time and allow taking temporal changes, such as vehicle rerouting, into account (Chang et al., 2012; Nojima and Sugito, 2000). They are more realistic, but take more time to execute compared to static traffic models. Chang et al. (2012) for example only analyzes 25 nodes and 75 links while Nojima and Sugito (2000) analyzed 100 links and 30 nodes. There is currently a gap in extending the benefit of dynamic traffic analysis to large spatial-scale networks while retaining results on not only the highways but also the local roads for a complete assessment of the mobility situation. This is particularly a problem for post-hazard traffic assessment, where the impact of infrastructure damage may propagate to a whole region. In such cases, the local roads serve as important links to ensure the basic level of mobility required after a hazard.

2.3 RESILIENCE AND PERFORMANCE ASSESSMENT

Measuring a transportation network's performance under seismic hazards can generally be divided into two types: those pertaining directly to transportation effects and those that pertain to external and indirect impacts. The first type includes metrics such as the total number of fulfilled trips (which indicates the connectivity of the post-earthquake network), changes in travel times, changes in trip length, and overall resilience and recovery speed of the network (Suarez et al., 2005; Wu et al., 2021; Chang et al., 2012; Nojima and Sugito, 2000; Feng et al., 2020). Almost all prior studies include consideration of these performance metrics. As mentioned in the previous section, impacts on transportation spill over to other sectors due to the interdependency of these critical infrastructures. Examples of this indirect performance metric include measures of safety (Wu et al., 2021), accessibility of hospitals (Feng et al., 2020) and businesses, and economic losses (Cho et al., 2001).

As both time and money are limited but crucial resources in mitigating earthquake impacts, it is important to deeply examine the potential economic impacts of hypothetical earthquakes on the transportation network and make adjustments accordingly. Many studies focus on rehabilitation strategies or prioritization of bridge retrofitting based on importance (Bhattacharjee and Baker, 2021; Wu et al., 2021; Frangopol and Bocchini, 2011; Dong et al., 2014) without explicitly considering economic impacts or the time and financial constraints. Estimating economic impacts aids in understanding the current resilience of the network with a more concrete figure. This, in turn, informs the formulation of more realistic policy recommendations, such as bridge repair prioritization or instead reallocating resources to tasks like building retrofits or enhancing hospital and emergency response capacities, based on the resilience assessment results. Alternatively, these results can also help in understanding the risks associated with delaying highway and bridge restoration or maintenance in the event of an earthquake.

Other studies have examined the economic impact of seismic hazards on different levels. The most common of these studies is through the use of input-output (I-O) analysis as popularized by Leontief (1986). This method uses an input-output table that summarizes all interactions between each pair of sectors in a given region. This can then be used to show how any change in economic activity in one sector can result in ripple effects to others (Brookshire et al., 1997). Another method of quantification is to measure the overall economic impacts using integrated transport networks and multiregional trade models (Ham et al., 2005). This entails collecting commodity flow data to and from each zone of analysis. While the US Bureau of the Census and the Bureau of Transportation Statistics collects this data between the 50 states and smaller regional economic units, the granularity may not be fine enough if the objective is to assess the local economic impacts of an earthquake. Computable General Equilibrium (CGE) models are another popular way of measuring economic impact as they incorporate the behavior of producers and consumers to price signals, on top of allowing nonlinearities as opposed to I-O models. However, the same data availability issues hinder the use of CGE models as employed in Tatano and Tsuchiya (2008). While these methods offer comprehensive analyses, it is difficult to develop an understanding of more specific effects to individual sectors like transportation. Furthermore, the granularity of

results from impact analyses at this overall regional level of abstraction is not fine enough to make specific conclusions, actionable items, and strategies at the transportation sector level.

Of the three mentioned components of resilience analysis of transportation networks to seismic hazards (bridge modeling, traffic modeling, and performance/resilience metrics, including economic losses), different studies have not applied all three consistently. Cho et al. (2001) is the best example of applying all these steps, but each step, particularly that of the transportation network model and economic model, is still wanting in terms of granularity. Therefore, a considerable gap also exists in calculating the economic impact on the transportation sector on a more granular level of analysis, both on the bridge and traffic modeling sides.

2.4   GAPS TO BE ADDRESSED

The preceding literature review uncovers four main gaps: First, previous bridge modeling studies under seismic hazards have largely used assumptions to group bridges into classes to simplify analysis and have not utilized satellite images and other newer sources of data to make more individualized models. Second, previous traffic models have largely had to make a choice between (a) macrosimulation/static models or microsimulation/dynamic models, and relatedly, (b) large networks or small networks. This has led to studies that either focus on a regional perspective without much insight on local effects or a local perspective without much insight on regional effects. Third, while there have been a few studies that looked into the socio-economic impact of earthquakes to the transportation system and its users, they largely also suffer from the choice between regional or local impacts and are at times proprietary and inaccessible. Lastly, there is a gap in studies that address all the aforementioned issues in a singular framework.

The goal of this report therefore is to provide a synthesis approach that: (1) factors in the different structural and seismic characteristics of individual bridges across the regional scale using an efficient image-based structure-and-site-specific fragility generation method, combined with (2) a large-scale/ regional, agent-based semi-dynamic traffic simulation that can then lead to (3) disaggregate cost, resilience, and economic impact assessments attributable to individual system components/aspects (e.g., local roads vs highways; reroutes, delays vs trip cancellations), all in all, to extract highly granular information that can guide the formulation of resilience assessments and preparation plans with both local and regional perspectives taken into account.

The remainder of this report is organized as follows. Section 3 introduces the proposed framework and the methodologies in detail. In Section 4, a case study of the framework applied to the Los Angeles region is presented. In Section 5, the results from the regional simulation case study are discussed, including the direct transportation interruption metrics as well as the economic impacts. Section 6 provides a summary of the study and suggestions for future studies.

3   METHODOLOGY FRAMEWORK

A four-step framework is adopted to facilitate the inclusion of highly granular infrastructure seismic performance in this study. Compared to existing methods as reviewed in the literature, the adopted framework components have the advantages of being efficient and scalable, which facilitates the inclusion of detailed bridge- or road link-level results for nonetheless large-scale system-level analysis. A detailed flowchart of this framework is shown in Figure 3.1. In this section, the focus is given to the latter three steps (bridge assessment, transportation network analysis, and economic impact analysis), highlighting their granularity and applicability to regional analysis. The hazard characterization method follows Koc et al. (2020) and Cetiner (2020) where for seismic hazards, first, a scenario earthquake is identified, followed by the use of ground motion prediction equations (GMPEs) to get Intensity Measure (IM) outputs, such as peak ground acceleration (PGA), peak ground velocity (PGV), and peak ground displacement (PGD) which are then used as inputs to the subsequent bridge modeling methods.

3.1   BRIDGE MODEL GENERATION AND DAMAGE ASSESSMENT

For this study, bridges are considered the only vulnerable components of the transportation network, given their higher likelihood of sustaining damage requiring extended time frames for full recovery, as evidenced by historical major seismic events (Cooper et al., 1994; Kawashima and Buckle, 2013), and the limited disruption potential of the other transportation components, at least using HAZUS fragility functions (FEMA, 2003). In order to establish a detailed representation of the structural and seismic characteristics for individual bridges in a large geographical area, the image-based model generation methodology proposed by Cetiner (2020) is used. This approach consists of five high-level steps:

1. Identifying tentative bridge locations for a region from National Bridge Inventory and refining this location information using an OpenStreetMap and routing APIs,

2. Downloading all street-level imagery associated with each detected bridge,

3. Reconstructing 3-D bridge geometry for each bridge using the downloaded imagery,

4. Populating these geometric shells with structural information using class statistics to develop nonlinear bridge models,

5. Calculating bridge fragility functions using component damage thresholds available in the existing literature.

The first step, identifying bridge locations and centerline geometry, begins with extracting approximate coordinate information available in the National Bridge Inventory (NBI) (FHWA, 1995). Once these coordinate values are obtained, all bridge centerlines that are within a mile

radius of NBI coordinates are detected using OpenStreetMap (OSM)'s Overpass API[3], and the bridge geometries that match the route information stated in NBI are retained. Subsequently, to narrow down the query to a single unique matching centerline, a navigation query from the beginning and end vertices of each centerline curve is generated using Google Directions API[4], and the route/direction information for a bridge centerline that match NBI route and direction information is selected.

Benefiting from the unique strengths of each data source, this process results in accurate centerline extractions. NBI contains precise location and route information for every bridge in the US but lacks the centerline information captured in OSM. OSM, on the other hand, has accurate centerline polygon and route information[5] but lacks the direction information needed, e.g., northbound or southbound, to match these polygons to NBI bridges. Google Directions API provides detailed routing information between two points but is somewhat limited in the accuracy of the path connecting these points. By combining these three sources, the centerline geometry of a bridge and the facility it carries is easily identified.

To download the street-level images for each bridge, two curves offset from the bridge centerline by a distance proportional to the NBI length of the bridge are computed. Next, all the Google Street View imagery on or near these curves is harvested, keeping track of the camera locations of images as they are obtained.

The street-level imagery for each bridge is semantically segmented using a deep learning model utilizing DeepLabV3 architecture (Chen et al., 2018) to identify all image regions containing bridge bent and deck elements. Then, the unique columns in each image and their locations are determined based on their order of occurrence and their linear distance along or offset from the bridge centerline. At this step, images for each unique column are grouped separately to determine column dimensions. By running the end-to-end wireframe parsing model by Zhou et al. (2019) on column masks of segmented images, the vertical column lines are identified; counting the number of these vertical edges, column shapes are determined (e.g., two edges if circular, three edges if rectangular). Camera parameters at each column location are extracted using the multi-view automatic calibration pipeline developed by Vasconcelos et al. (2018). Subsequently, the heights and widths of each column are sampled at numerous intervals to determine the column dimensions. Superstructure depth is measured as the normal distance between the bottom and top faces of the

---

[3] OpenStreetMap, 2022. OpenStreetMap. https://www.openstreetmap.org.

[4] Google, 2022. Google Directions API.
https://developers.google.com/maps/documentation/directions.

[5] US Census Bureau, 2021. Tiger/line shapefiles. URL:
https://www.census.gov/geographies/mapping-files/time-series/geo/tiger-line-file.html.

superstructure. The top width of the bridge deck is read from the relevant NBI field, and the bottom is extracted from auto-calibrated images.

By the end of this step, a three-dimensional geometric model for each bridge is established. To convert these geometric models into structural models, the class statistics by Mangalathu (2017) are utilized. For bridge columns, the longitudinal and transverse rebar locations, as well as concrete and steel strength properties, are computed based on the era-specific rebar ratios and strength distributions (where the construction year of a bridge is obtained from NBI). Then, using this cross-sectional information and era-specific standard connection details, columns are modeled using force-based formulation as discussed by Neuenhofer and Filippou (1997). Spread of plasticity across column cross-section and length due to flexure are computed using a beam-column element with fiber sections where moment-curvature and axial force-deformation characteristics and their interaction are explicitly considered. Column shear behavior is considered by combining this beam-column element in series with the limit state uniaxial material suggested by Elwood (2004).

Abutments are modeled as zero-length elements that are assembled differently based on the abutments' construction type. The longitudinal behavior of integral abutments is modeled using springs with a tri-linear force-deformation relationship for the contribution of abutment piles, as presented by Mangalathu (2017), and a Generalized Hyperbolic Force–Displacement (GHFD) backbone curve for the passive resistance of the abutment backfill, as proposed and described by Khalili-Tehrani et al. (2016). In seat-type abutments, the lateral resistances of the abutment back wall and elastomeric bearings are also factored into the longitudinal resistance of the abutment. The seat back wall is modeled using the simplified impact model proposed by Muthukumar (2003), and the bearing pads are assumed to follow the elastic-perfectly plastic behavior suggested by Caltrans (2019). The transverse behavior of a diaphragm abutment is assumed to comprise the lateral resistance of abutment piles alone, with the pile behavior defined as identical to the longitudinal behavior. In defining the abutment resistance in the transverse direction for seat-type abutments, however, the resistances of elastomeric bearings and shear keys are also considered. Bearings are assumed to follow the elastic-perfectly plastic force-deformation relationship identical to that prescribed in the longitudinal direction. The transverse resistance of each shear key is defined as the shear resistance from the shear key reinforcing steel and concrete combined in parallel as per Silva (2009) and connected in series to an elastic no-tension material to account for the gap between the deck and shear keys. Similar to the application for bridge columns, the statistical properties of all the lateral pile, elastomeric bearing, and soil resistances required to define the described abutment models were obtained from Mangalathu (2017).

The superstructure is assumed to remain elastic under earthquake shaking. Hence, elastic properties based on the gross area of the superstructure are assigned to line elements representing the superstructure. For scalability of this nonlinear modeling approach, all bridge models are generated using OpenSees (McKenna, 2011) through custom-built automation scripts.

The relationship between the probability of each bridge reaching or exceeding different damage states for an earthquake intensity measure (IM) is defined using fragility functions. In certain situations, to account for different seismic conditions, multiple sets of fragility functions may be

derived for different IMs (e.g., to account for ground shaking and ground failure-induced damages to bridges, two sets of fragility functions may be defined in terms of the IM's of 1-second spectral acceleration and peak ground deformation, respectively). Following performance-based earthquake engineering (PBEE) methodology (Moehle and Deierlein, 2004a), fragility functions are prescribed as lognormally distributed functions and are generated for four distinct damage states: slight (ds_1), moderate (ds_2), extensive (ds_3), and complete (ds_4). Each fragility function is characterized by a median value IM (M), and a lognormal standard deviation value (β). The general form of a fragility function according to Baker et al. (2021) is

$$\Pr\left(D^k \geq ds_j \middle| \mathrm{IM} = x^k\right) = \Phi_j^k\left(\frac{\ln\left(x^k/M\right)}{\beta}\right) \tag{3.1}$$

where k is the index of the IM for which the fragility function is established (e.g., for the case study discussed in the following section, only one IM is utilized; hence, the superscript k can be ignored in defining fragility functions), j is the PBEE damage state index, D^k is the damage state of a network component due the kth IM being equal to x^k, x^k is the value of the kth IM at the site of the network component, and Φ is the normal cumulative distribution function with parameters M and β. Here, the no damage state is denoted as ds_0. The component threshold values required to develop these fragility curves were defined as outlined by Ramanathan et al. (2015). The fragility functions were computed via multiple-stripe analysis (Jalayer and Cornell, 2009) using the ground motion record sets developed for the Pacific Earthquake Engineering Research Center, Transportation Research Program (Baker et al., 2011).

To calculate the total functionality level of a network component, it is necessary to determine the probabilities of this component being in each of the five damage states for a set of IMs (P_j^k) as below.

$$P_j^k = \begin{cases} \Pr\left(D^k \geq ds_j\right) - \Pr\left(D^k \geq ds_{j+1}\right), & j = 0,1,2,3 \\ \Pr\left(D^k \geq ds_j\right), & j = 4 \end{cases} \tag{3.2}$$

where $\Pr(D^k \geq ds_0) = 1$.

Once these P_j^k values are combined with the restoration functions suggested by FEMA (2003) for each damage state RC_j as follows, the total functionality level FL of a network component due to the kth IM can be computed.

$$FL^k = \sum_{j=0}^{4} P_j^k \cdot RC_j \tag{3.3}$$

3.2   TRANSPORTATION NETWORK ANALYSIS

To capture the effects of bridge damage on the traffic network performance at a large geographic scale, an open-source agent-based semi-dynamic traffic assignment model developed at UC Berkeley (https://github.com/cb-cities/residual_demand) is adopted (Zhao et al., 2019; Chan et al., 2021). The traffic model takes in two types of inputs: as the first input, on the road network supply

side, the base road network information is downloaded from OSMnx (Boeing, 2017). The network structure is represented by the nodes (i.e., road intersections) and links (i.e., stretches of road between two intersections). Various traffic-related attributes are attached to the road links, such as the length, speed limit, and capacity. On the travel demand side, a list of time-stamped OD pairs is taken as the input, which can usually be obtained or extracted from the local travel demand surveys or models.

Given the network supply and travel demand inputs, the traffic assignment module is then initialized: the simulation starts at 12 AM when there is relatively light traffic on the road network. With a time step of 15 minutes, vehicles (time-stamped OD pairs) with a departure time between 12 - 12:15 AM are incrementally assigned (100,000 ODs at a time) the initial fastest paths based on free-flow traffic conditions. The incremental assignment here increases the stability of the results by avoiding all vehicles getting assigned to the same routes. After each increment, the traffic congestion status is updated for the network, and a new travel time is calculated for each link using the Bureau of Public Roads (BPR) volume-delay curves (USBPR, 1964) as shown in Equation 3.4, modified to take into account traffic signal and crossing delays:

$$t_i = t0_i * \left(1 + \alpha * \left(\frac{v_i}{c_i}\right)^{\beta}\right) + \text{traffic signal delay} + \text{crossing delay} \qquad (3.4)$$

where t_i is the travel time on link i, $t0_i$ is the free-flow travel time on link i, v_i is the flow on link i, c_i is the capacity of link i, and α and β are calibration parameters set to the commonly used value of 0.6 and 4, respectively (Colak et al., 2016). Traffic signals and crossing delays are also taken into account as this information is also provided by OSMnx.

An intermediate stopping location is determined for each vehicle that cannot finish the journey within the 15-minute interval. The intermediate stopping locations will then be set as the new origin to allow vehicles to reroute (e.g., choosing a more optimal path) based on an updated traffic congestion status and finish the journey in the subsequent time steps. Such incremental assignment and residual demand calculation procedures are repeated for each 15-minute interval until 12 AM the next day. The outputs include both vehicle-level information (travel time) and link-level information (traffic volume per 15-minute interval). Many summary statistics, such as the Vehicle Miles Traveled (VMT) and Vehicle Hours Traveled (VHT) can thus be derived from this output.

Each agent is assumed to be selfish, i.e., choosing the path that would minimize their individual travel time, and having perfect information on the traffic conditions, which includes the changes in travel time on each link in the network due to congestion. This is possible due to the incremental loading (100,000 ODs at a time) of the network and the iterative calculation and link travel time and route choice every 15-minute interval. As such, user equilibrium is approximated in this model. While there are arguments that post-earthquake scenarios are not necessarily in equilibrium due to the uncertainty and the damage (Nikoo et al., 2018), it is adopted in this model as a conservative estimate of loss (i.e., assessing the impacts to trips that could normally have been fulfilled).

The traffic model has been adapted here to capture the effects of bridge damage. Specifically, for damaged bridges (and surrounding or underlying roads that cannot be accessed), the traffic model will label them as "closed links". For these closed links, they are assigned extremely small speed limits and capacity, which effectively leads to extremely high travel times (e.g., over 10 hours) for vehicles using them. In the simulation code, a supplementary logic is implemented to check the travel time of each assigned route. If the route travel time is over a certain threshold, the route must have gone through one of the closed links, and no faster path exists. The trip is then labeled as "unfulfilled". It is expected that more trips will be unfulfilled with increasing bridge damage severity.

If additional information, such as different trip activities and different vehicle types, are available, each agent can be labeled and restricted accordingly in the simulation for a richer analysis later on.

3.3   ECONOMIC IMPACT ESTIMATION

The economic cost of damages in a transportation network is estimated by splitting it into two components: direct costs and indirect costs, as shown in Equation 3.5 (Moehle and Deierlein, 2004b).

$$C = C_{direct} + C_{indirect} \tag{3.5}$$

Direct costs associated with bridge b are computed based on the amount of resources needed to repair the damaged road components in the network as shown in Equations 3.6 and 3.7, where RCR is the repair cost ratio and A_b is the area of the bridge b (Bhattacharjee and Baker, 2021). The unit replacement cost is \$3,154 per square meter (Federal Highway Administration, 1995).

$$C_{direct} = \sum_{b=1}^{B} C_{direct}^{(b)} \tag{3.6}$$

$$C_{direct}^{(b)} = 1^{(b)} * \text{RCR} * A_b * \text{unit replacement cost} \tag{3.7}$$

On the other hand, indirect costs incurred over the time period when road components are damaged can be further split into two components: costs due to delays to the travelers, and costs due to lost demand or unfulfilled trips as shown in Equations 3.8 and 3.9 (Bhattacharjee and Baker, 2021).

$$C_{indirect} = C_{delays} + C_{connectivity} \tag{3.8}$$

$$C_{indirect} = \alpha \Delta T + \gamma U \tag{3.9}$$

where α is the value of travel time and γ is the value of productivity. ΔT is the change in total travel time, and U is the number of unfulfilled trips, both relative to the base pre-earthquake scenario. α and γ vary for each region and can be computed using Equations 3.10 and 3.11 (Bhattacharjee and Baker, 2021).

$$\alpha = \frac{\text{Median household income, USD}}{2080 \text{ h worked per year}} \tag{3.10}$$

$$\gamma = \frac{\text{Annual gross regional product}}{\text{Annual labor hours}} \tag{3.11}$$

Once cost estimates are obtained, they can be compared with other economic and financial measures such as the gross domestic product (GDP) of the area to get a sense of its scale compared to the economy at large, or the allocated budgets for bridge repair and restoration or seismic retrofitting by the Department of Transportation on the state or federal level.
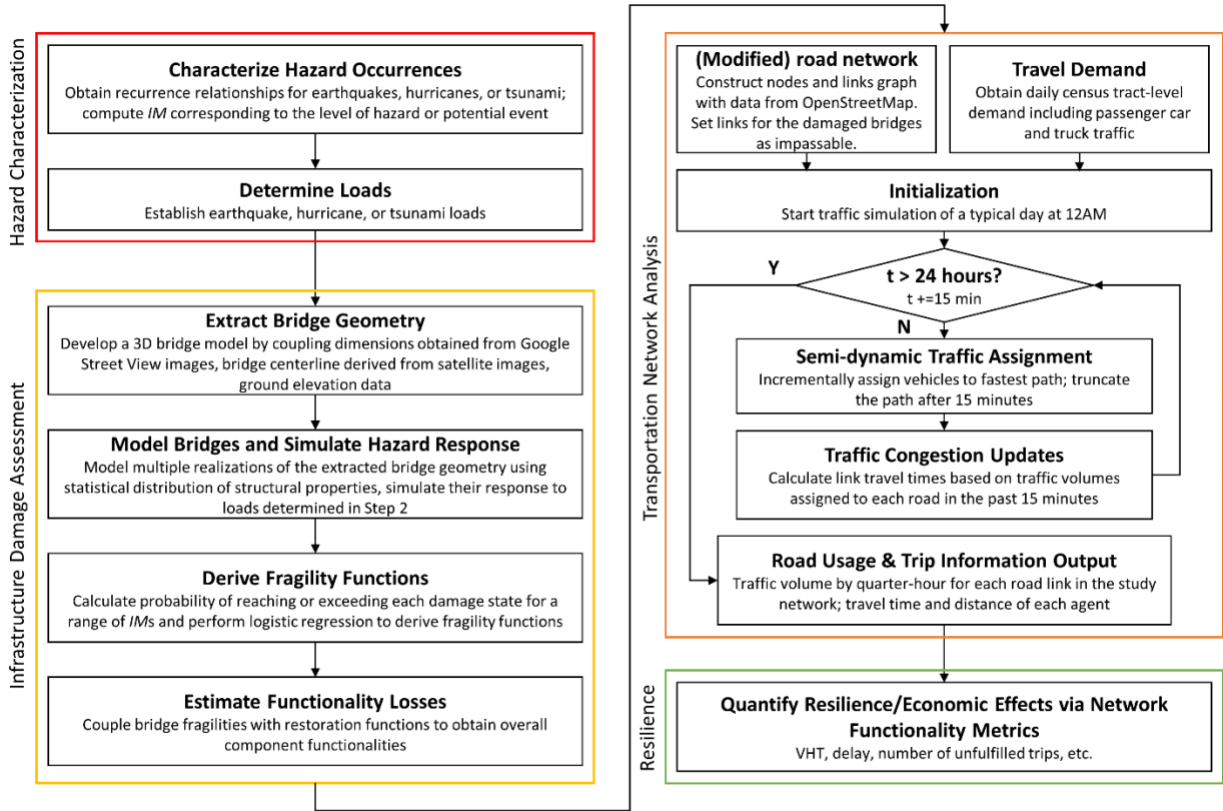
CHAPTER 3: FIGURES

Figure 3.1   Flowchart of the developed methodology.

4 CASE STUDY: SOUTHERN CALIFORNIA (PORTS OF LOS ANGELES AND LONG BEACH)

To more clearly highlight the contributions of our framework, we apply it to a case study in and around the Los Angeles port area.

4.1 HAZARD CHARACTERIZATION AND INFRASTRUCTURE DAMAGE ASSESSMENT

Nonlinear structural models were developed for 1,000 bridges around the Ports of Los Angeles and Long Beach (POLA/POLB) using the automated image-based approach introduced in Section 3.1. The expected 1-second spectral accelerations at each bridge site were obtained using the physics-based approach proposed by Southern California Earthquake Center (Small et al., 2017) for a M_w 7.4 Palos Verdes Fault scenario event, two miles off the port islands as shown in Figure 4.1. Spectral acceleration at 1.0 s is selected as the IM of use in this study due to its high sufficiency and proficiency ratings determined by Shafieezadeh et al. (2012) and its ease of use over vector-valued or fractional order IM definitions for representing ground shaking effects (ground shaking is the expected primary driver of seismic damage for the study area). Expected damage probabilities and functionality levels, together with the required recovery time of the bridges, were determined for the computed 1-second spectral accelerations. Figure 4.2 shows the fragility functions computed for two of the bridges modeled for this study. Figure 4.3 shows the road closure map using the proposed method. For the purposes of this study any bridge with a functionality less than 75% was deemed fully closed for traffic, as defined in Gordon et al. (2004) (no partial bridge closure condition was considered). Furthermore, once a bridge is closed, all road segments feeding traffic into, or underlying, this bridge will also be closed for traffic. In this road closure map, 59 miles of roadway were predicted to be closed the day after the scenario earthquake, 44 miles of roadway remained closed 3 days post-earthquake, 14 miles of roadway remained closed 7 days post-earthquake, 10 miles of roadway remained closed 14 days post-earthquake, and 6 miles of roadway remained closed 30 days post-earthquake. This road closure map is used as the input to the subsequent transportation network analysis.

4.2 TRANSPORTATION NETWORK ANALYSIS

4.2.1 Road network data

Road network data for six counties in Southern California represented by the Southern California Association of Governments (SCAG) has been gathered from OSMnx. The network is converted

into a directed graph representation consisting of 1,444,790 edges and 615,174 nodes where each edge represents a directed road segment and each node represents a road connection or intersection.

4.2.2 Travel demand data

Inter-traffic analysis zone (TAZ) origin-destination data in normal situations (i.e., without earthquake damage) was also obtained from SCAG. Processing this data led to a total of 42,056,426 trips in the whole SCAG region for a typical day composed of 40,814,733 car trips and 1,241,693 truck trips. Table 4.1 shows the travel demand summary for each time of day, while Figures 4.4a and 4.4b show visualization of the overall travel demand and the port travel demand.

While Khademi et al. (2015) suggested that travel demand substantially changes post-earthquake and thus employed hundreds of person-hours of experts to determine the new travel demand, it is difficult to do this for most scenarios. In this paper, we use the same travel demand pre- and post-earthquake, but we anticipate that a number of trips will not be completed in the post-earthquake simulation scenarios due to a lack of connectivity in the network. This uncompleted/unfulfilled trip metric will be reported in the results in Section 5.

Sampling. Due to the computationally intensive requirements of this kind of traffic simulation, we decided to sample the origin-destination data such that 1 agent represents 5 vehicle trips. The final simulation input is composed of 8,158,000 car agents and 246,218 truck agents for a total of 8,404,218 agents. The output figures are also adjusted accordingly with a factor of 5.

4.2.3 Traffic simulation

The agent-based semi-dynamic traffic assignment model introduced in Section 3.2 is used to compute the sub-hourly changes in road usage. Each trip is assigned an initial route based on the computed shortest path using contraction hierarchies from origin to destination (Foti et al., 2012). Each edge's volume is updated every 15 minutes and each trip's shortest path is recomputed based on the new network congestion status. Trucks were restricted from traveling on residential roads.

Six scenarios were simulated: (1) a base scenario with no road closures, (2) a scenario 1 day post-earthquake, (3) a scenario 3 days post-earthquake, (4) a scenario 7 days post-earthquake, (5) a scenario 14 days post-earthquake, and (6) a scenario 30-days post-earthquake. Each post-earthquake scenario includes road closures from the bridge damage analysis in Section 4.1. Each simulated scenario yields three main outputs: the traffic volume at each link for every 15 minutes of the simulation, the total travel time of each agent, and the total trip distance of each agent.

Due to the bridge modeling output being a deterministic set of bridges for each scenario, the simulations are not expected to produce vastly different results for each run with the same input and scenario parameters. However, each scenario was run 10 times to rule out the impact of possible random variations in each run (e.g., sequence in which shortest path is calculated for each agent, selection among multiple shortest paths). For each scenario, the average of metrics such as travel time and travel distance over 10 runs was taken and used these averages as the main results

for analysis. The variations, or lack thereof, in the results generated from these random repetitions are reported in Section 5.2.

CHAPTER 4: TABLES

Table 4.1   Travel demand summary.

Time of day	# of car trips	# of truck trips	Total trips
6am - 9am	7,396,597	201,815	7,598,412
9am – 3pm	15,146,975	504,754	15,651,729
3pm – 7pm	12,036,376	219,119	12,255,495
7pm – 9pm	3,117,935	69,886	3,187,821
9pm – 6am	3,116,850	246,119	3,362,969

CHAPTER 4: FIGURES
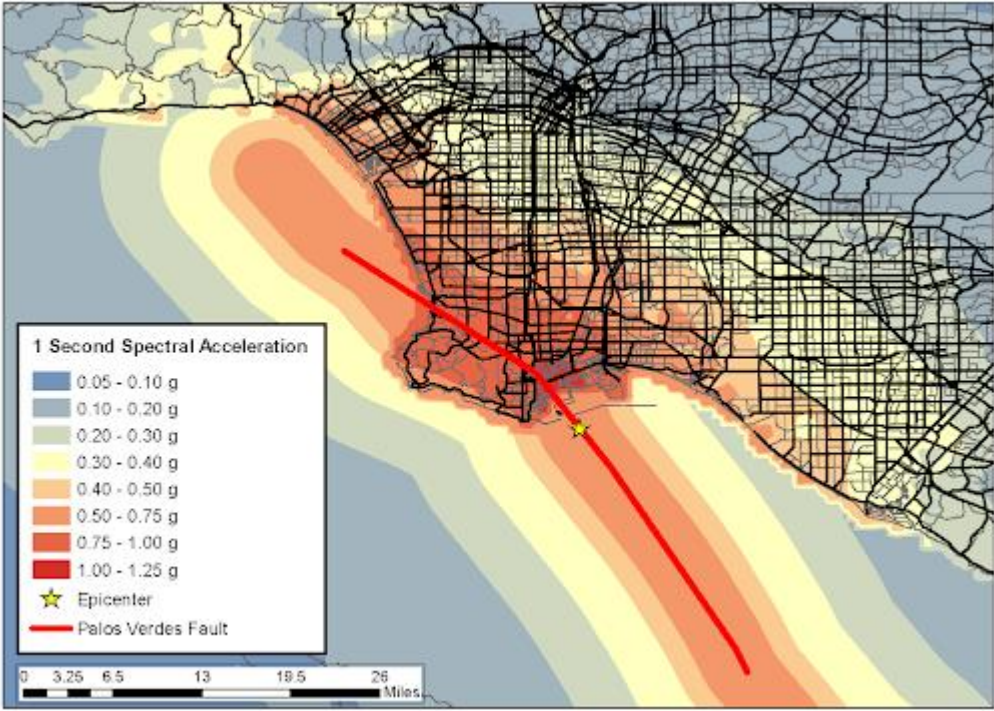
Figure 4.1   Sample earthquake visualization from Cetiner (2020).
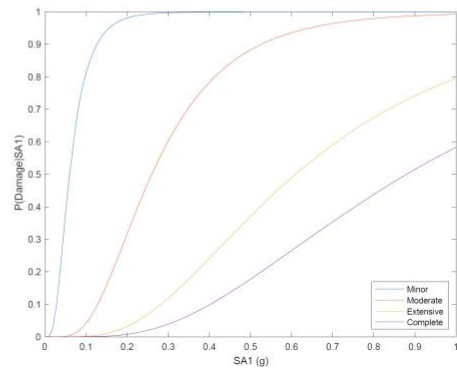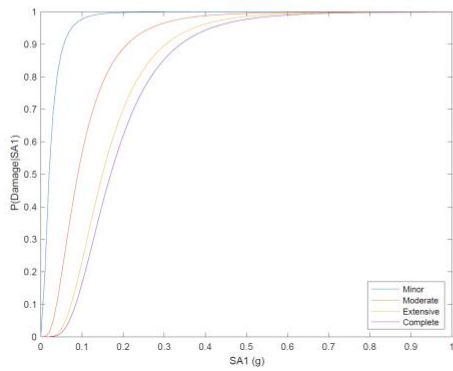
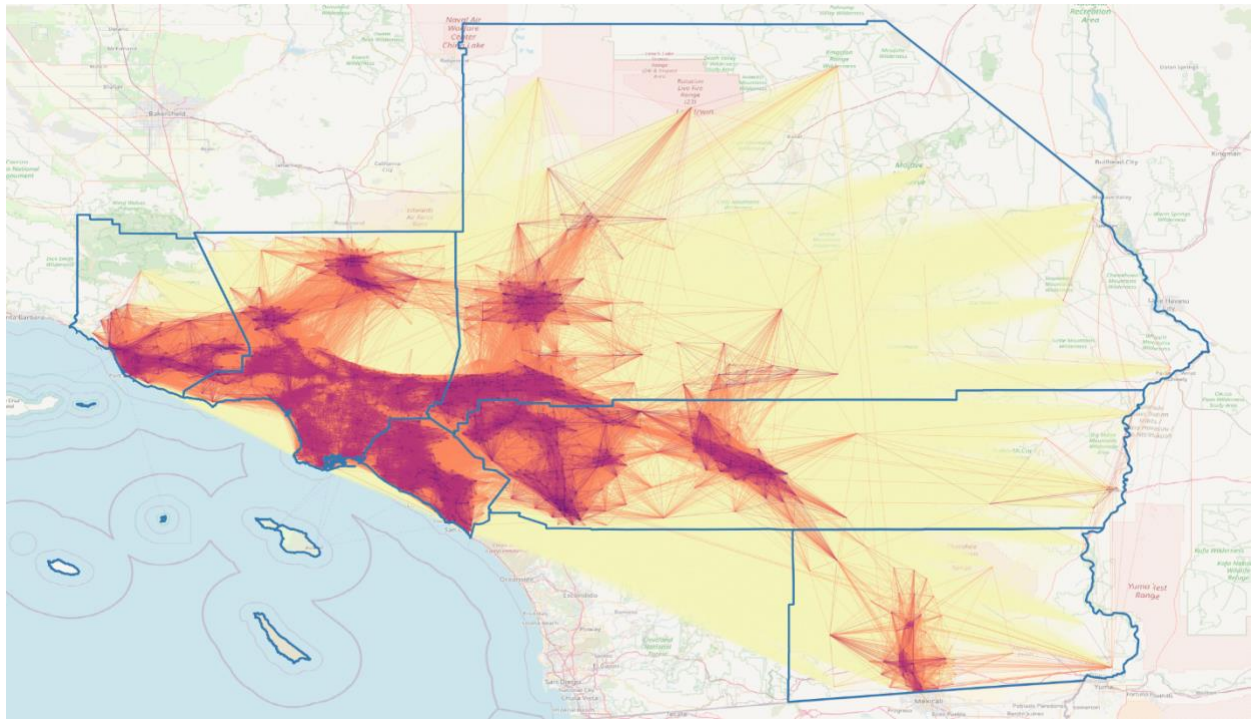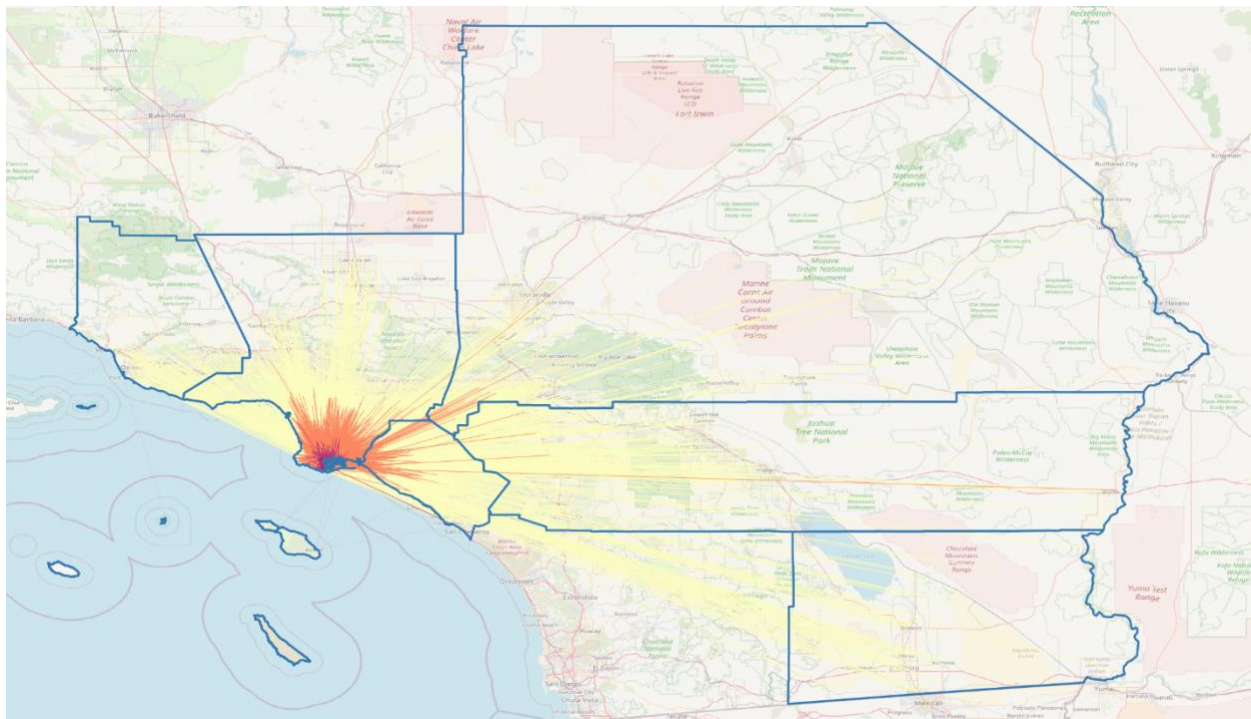**Figure 4.2   Fragility functions computed for two of the modeled bridges.**
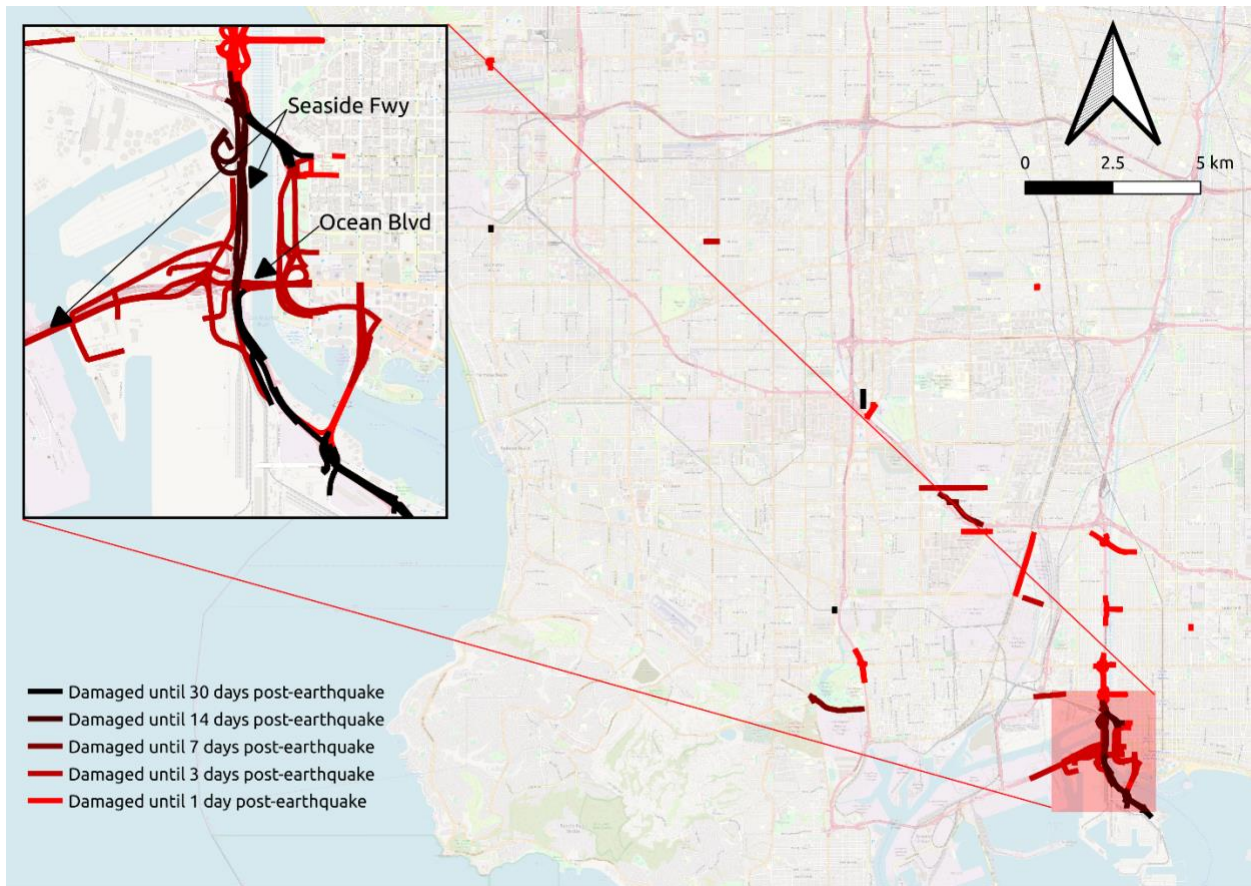
Figure 4.3   Road closure map.

(a) Overall travel demand

(b) Port travel demand

Figure 4.4   Travel demand data.

5   RESULTS AND DISCUSSION

5.1   INITIAL VERIFICATION COMPARED WITH REAL-LIFE METRICS

To assess the performance of our model framework, some metrics in the Southern California Association of Governments (SCAG, 2020) Transportation Plan, that are comparable to our model outputs, were utilized. Some of these key metrics are:

- **Mean commute time:** SCAG lists the mean commute time—defined as the average travel time to work—as 32.1 minutes. Our input data on travel demand (in Section 4.2.2) does not have activity labels (work/non-work) but the average travel time computed for the base scenario from our simulation for all trips is 29.4 minutes.

- **Average distance traveled:** SCAG lists the average distance traveled as 17.9 miles for work trips and 5.8 miles for non-work trips. The base scenario leads to an overall average travel distance of 15.1 miles, which is within the SCAG range.

- **Percent of trips less than 3 miles:** SCAG states that 14.0% of work trips are less than 3 miles while 40.5% of non-work trips are less than 3 miles. The base scenario computes 26.1% of all trips being less than 3 miles, which is also well within the SCAG range.

From these key metrics, it was concluded that the traffic model resembles the real-life transportation scene in general despite the lack of activity labels on existing data. The availability of activity/trip purpose labels in travel demand inputs can greatly enrich model assessment in future studies.

5.2   ROBUSTNESS TO RANDOM VARIATIONS

Average travel time variation across random seeds (base scenario) varies between 29.32 to 29.37 minutes (around 0.05 minutes or 3 seconds as shown in Figure 5.1), which is much smaller than the increase from the base to Day 1 scenario that can be seen in Figure 5.3c. We, therefore, do not expect randomness across simulations to be significant enough to impact our overall results.

5.3   PORT AREA ANALYSIS

Focusing on the port area, we aggregate these trip time and distance outputs for each agent to get the overall vehicle hours traveled (VHT), average travel time, and the number of fulfilled & unfulfilled trips for each post-earthquake scenario relative to the base scenario, as shown in Table 5.1. A trip is labeled as *unfulfilled* if the vehicle is unable to travel from its origin to its destination due to damage to the road network.

Figure 5.2 shows the general steps taken to interpret the results obtained for the port area to understand the changes in travel-related metrics at different stages of the earthquake recovery. The primary indicator used to assess the level of impact to the transportation network is the overall vehicle-hours traveled (VHT). Figure 5.3a shows the trend in total VHT for the port area trips. In the base scenario, the VHT is 199,592 vehicle-hours. After the hypothetical earthquake, there is a 10% decrease from Day 0 to Day 1, coinciding with the worst bridge damage and road closure scenario. Despite 14 miles of roadway reopening immediately after Day 1, a small but unexpected 2.5% decrease in VHT happened from Day 1 to Day 3, which makes the VHT to be at the lowest point on Day 3 at 175,272 vehicle-hours, or 12.5% reduction compared to the baseline. From Day 3 on, the VHT starts to recover: a relatively big increase in VHT is observed from Day 3 to Day 7. From Day 7 to Day 30, the VHT plateaus at around 192,843 vehicle-hours, a 4% decrease relative to the base scenario.

To understand the trends in VHT, two components that are influential to VHT are examined: the change in the number of fulfilled trips (completed trips) and the change in the average travel time. The former indicates changes in the connectivity of the road network, as a more severely damaged network would lead to more trips being unable to finish. Figure 5.3b shows the trend in the number of fulfilled trips starting or ending in the port area. There is a steep drop from Day 0 to Day 1 with 15% of port trips unable to be completed; this minimum coincides with the worst bridge damage scenario right after the earthquake, in particular, attributable to 39 bridges and 59 miles of roadway being closed on key access ways within 15 miles of the port. A small recovery in the trip fulfillment rate is observed on Day 3, due to the recovery of 16 bridges that are mostly external to the port area. The biggest recovery of the trip fulfillment rate happened on Day 7. This large increase in fulfilled trips on Day 7 is due to the reopening of the western portion of the Seaside Freeway bridge that connects the western and eastern sides of the Port of Long Beach and the Port of Long Beach island to the mainland (see Fig. 4.3). Slow but steady recovery of the trip fulfillment rate is observed throughout to Day 30 when the number of unfulfilled trips is still about 4% of total port trips a month after the earthquake with 10 bridges and 5.5 miles of roads predicted to be still closed.

On the other hand, changes in the average travel time (calculated only for fulfilled trips) indicate a vehicle's need to detour due to closed roads. Figure 5.3c shows the trend of the average travel time of trips starting or ending in the port area. The average travel time increases by 6% from Day 0 to Day 1, indicating that trips still able to be completed took a longer time to do so, also coinciding again with the worst damage scenario as expected. Average travel time decreases much closer to baseline on Day 3 (with an increase of only 1.7% relative to baseline) when 16 out of 39 damaged bridges are reopened. The average travel time steadily decreases through Day 30 as more bridges are reopened and it is almost similar to that of the base scenario.

These trends are mostly intuitive except for the slight drop in the overall VHT from Day 1 to Day 3. Figures 5.3c and 5.3b respectively show that the average travel time decreases on Day 3, but the number of fulfilled trips only increases incrementally. This slight drop in overall VHT, therefore, shows that the change in the travel time component (averaged over 210,335 trips) dominates over the change in fulfilled trips (37,230 unfulfilled trips). This can be attributed to the opening of a road local to the port area that helps the vehicles avoid detours (thus reducing the travel times of

trips which can be fulfilled), while roads connecting the port area to the outside area are still closed and only start to open on Day 7. This kind of insight is one that can be made because of the resolution of the traffic simulation and its agent-based nature.

Another observation that stands out is that the increase in average travel time, at worst, is only 3 minutes. While this may seem small, it is important to note that this only takes into account delays due to the road closures because of the earthquake. Any congestion delays already present in the baseline scenario are not separated in this report, and therefore, the actual delays will be larger than 3 minutes. Regardless, these results demonstrate the resilience of the transportation network in the studied area. Furthermore, the averaging of the changes in travel time hides a slightly disproportionate impact on certain trips. Figure 5.4 shows the distribution of travel times of vehicles starting or ending their trips in the port area for Day 0 and Day 1. The shape of the distributions is mostly similar, which indicates that most trip travel times stay the same. To be specific, 75% of Day 1 trips stay within 10% of their Day 0 travel time. However, over 5% (around 5000) of trips have increases of 50% of their Day 0 travel time with some even increasing by a factor of 4 or more. Again, this kind of insight can be made because of the resolution of the traffic simulation and its agent-based nature.

5.3.1 Minimal changes in overall VHT but sizeable decreases in port VHT

Suarez et al. (2005) posits that the effect of hazards on VHT and VMT can be ambiguous. VHT, for example, can increase due to vehicles taking less straightforward trips on congested routes due to road closures, but can also reasonably decrease due to the reduced number of trips after a hazard. Figure 5.5 shows the changes in total VHT for the overall study area (orange line) and trips origin/end in the Port of Los Angeles area specifically (blue line). They show that, for this case study in particular, VHT changes negligibly for the overall study area over all of the post-earthquake scenarios. However, port VHT decreases by as much as 12%, indicating a sizeable decrease in productivity in the area. These big differences are attributed to the concentration of bridge damage in the port area, as 31 of the 39 damaged bridges (just under 80%) are within 3 miles of the port boundaries. These findings align with the above findings on changes in travel time.

5.4   ECONOMIC IMPACT ESTIMATION

Using the damage maps and simulation outputs from the previous step as inputs to Equations 3.5 through 3.11, the direct and indirect costs related to the transportation system in this hypothetical earthquake scenario are estimated. For direct cost calculations (costs to repair damaged infrastructures), it is assumed that the roads still closed on Day 30 will be repaired by Day 60, and

the repair cost ratio in Equation 3.7 is set at 0.68[6]. For the indirect cost calculations (economic losses due to delays or trip cancellations), the parameters are estimated from the regional economic statistics. For example, for the SCAG area, the median household income in 2018 was $64,989, which translates to an α of around $31 per hour of delay[7] in Equation 3.10. On the other hand, the gross regional product of California was $1,955,856 million in 2020 dollars and the number of labor hours was 25,101 million, which leads to a γ of $78 per hour per lost trip (Pabilonia et al., 2019) in Equation 3.11. The resulting value from Equation 3.5 indicates the estimated economic impact of the earthquake. The direct cost is calculated to be $1.56 billion while the indirect cost is calculated to be $768 million (only $121,000 of which is due to traffic delays due to very sparse closure throughout the overall LA region) for a total cost of $2.33 billion. For trips that start or end at the port area, the cost of lost demand dominates and is estimated to be at $476 million, while the delays cost $57,000.

5.4.1 Spatially disproportionate impacts

During hazards such as floods and earthquakes, the number of trips that are able to be completed is always expected to decrease (Suarez et al., 2005). This is true for our case study with there being as many as 73,845 trips (albeit less than 1% of the total trips) that are unfulfilled in the overall SCAG area one day after the earthquake, 37,230 (or 50% of all unfulfilled trips) of which start or end in the port area. As much as 62% of the total indirect cost is from the port area, showing the spatially disproportionate impact of the earthquake. This aligns with the finding that unfulfilled trips in the port area account for as much as 15% of all trips in the port area and is very evident in a spatial visualization of the area as shown in Figure 5.6.

5.4.2 Lost demand over delays

Additionally, the economic cost estimation shows that the impact of delays are dwarfed by that of lost demand (i.e., from the unfulfilled trips), as lost demand accounts for 99.98% of the computed indirect cost. Supporting this observation, Figure 5.7 shows that the economic recovery in the port area and the road restoration trend very similarly with time. Since the lost demand is a proxy indicator for the degradation of road network connectivity, this result shows that road network connectivity is the biggest issue post-earthquake in terms of the economic losses, while economic losses due to delays are relatively negligible.

---

[6] Federal Highway Administration, 2022. Bridge replacement unit costs 2020. https://www.fhwa.dot.gov/bridge/nbi/sd2020.cfm. Accessed: 2022-11-16.

[7] Southern California Association of Governments, 2019. Profile of the City of Anaheim. http://www.anaheim.net/DocumentCenter/View/13049/SCAG-Demographic-Profile-for-Anaheim?bidId=. Accessed: 2022-06-29.

5.4.3 Bridge closure costs versus bridge repair budgets

This study focused only on losses due to disruption to the transportation network, excluding seismic damage impacts to other port structures or buildings. This study also does not look into chain effects due to other sectors outside of transportation also being impacted. Because of this focus on transportation, the computed impacts cannot be directly compared to GDP which is based on a more comprehensive and general perspective of the regional economy. Instead, it is more appropriate to compare the results to budgets, both federal and state level, allocated for bridge repair.

For 2022, the federal government's Bipartisan Infrastructure Law granted California $574,785,473 under its Bridge Formula Program intended for bridge replacement, rehabilitation, preservation, protection, and construction. This is the first tranche under a five-year program with a budget of $4.2 billion[8]. However, the American Road and Transportation Builders Association (ARTBA) computes the total repair cost to be at $11.7 billion (American Road and Transportation Builders Association, 2022), more than half of which is not in the budget for the next five years. The computed costs of this hypothetical earthquake are a direct cost (due to repair/replacement of bridges) of $1.56 billion and an indirect cost (due to loss of demand and delay) of $768 million for a total of $2.33 billion. In the aftermath of an earthquake, this indirect cost can be taken as the amount of costs incurred by the individuals on top of federal/state bridge repair budgets brought about by a lack of pre-disaster mitigation. In other words, instead of only spending the direct cost of $1.56 billion to preventatively repair bridges before an earthquake, the cost increases by almost 50% post-earthquake which will largely be taken from each individual's personal income on top of taxes paid for the federal and state budgets.

It should be noted carefully, however, that the present study did not consider the direct seismic damage to port structures (wharves, cranes, container yards, etc.) due to ground shaking, or more importantly, the tsunami and inundation hazard, which could potentially close the entire port indefinitely. Impacts to the ports' productivity can also lead to cascading economic impacts that are more challenging to quantify. In the past years, the COVID-19 pandemic and a subsequent

---

[8] Caltrans, 2022. California to receive nearly $850 million in initial funding for bridge repair under federal bipartisan infrastructure law. https://dot.ca.gov/news-releases/news-release-2022-001#:~:text=California%20will%20receive%20%24849.4%20million,to%20address%20highway%20bridge%20needs. Accessed: 2022-11-16.

change in consumer behavior led to congestion in the ports and supply chain shortages[9,10,11]—the full impacts of which are yet to be studied. In effect, the estimates in this study are still conservative and would likely compound once other factors are considered.

5.5   IMPLICATIONS OF CASE STUDY

Figure 5.8 shows a representation of disaggregated cost based on our results. Due to the finer resolution of the methods used, the presented framework is able to come up with hierarchies of cost, as well as numerical estimates, that can be broken down between direct cost to repair or replace roads as opposed to socio-economic cost to the transportation system and its users. This can further be broken down spatially, for example between the port area and non-port areas, to focus on areas of interest. This can also be further broken down into car trips and truck trips because of the agent-based nature of our traffic model. With access to more data, these costs can be further broken down based on trip activity, demographics (such as age, sex, race), and more to analyze whether certain areas, groups, or sectors are affected differently compared to others or compared to the whole, and by extension, decision-makers are able to make more informed policy choices. This model can only improve with more granular information for bridges, roads, and trips.

---

[9] Dean, S., 2021. Is the ports logjam really getting better? the numbers don't tell the whole story. URL: https://www.latimes.com/business/story/2021-12-03/officials-say-the-ports-logjam-is-easing-but-numbers-dont-tell-the-whole-story.

[10] Isidore, C., 2021. Everything you're waiting for is in these containers. URL: https://www.cnn.com/2021/10/20/business/la-long-beach-port-congestion-problem-national-impact/index.html.

[11] The White House, 2021. Recent progress and actions on port congestion. URL: https://www.whitehouse.gov/briefing-room/blog/2021/11/10/recent-progress-and-actions-on-port-congestion/.

CHAPTER 5: TABLES

Table 5.1   **Port area measures.**

Scenario	[1] Total VHT = [2] * [3]	[2] Average travel time	[3] # of fulfilled trips	[4] # of unfulfilled trips
Baseline (Day 0)	199.59k veh-hrs	48.37 mins	247,565	NA
Day 1	179.75k veh-hrs	51.27 mins	210,335	37,230
Day 3	175.27k veh-hrs	49.19 mins	213,810	33,755
Day 7	191.49k veh-hrs	49.14 mins	233,785	13,780
Day 14	192.21k veh-hrs	48.98 mins	235,455	12,110
Day 30	192.84k veh-hrs	48.45 mins	238,795	8,770

CHAPTER 5: FIGURES
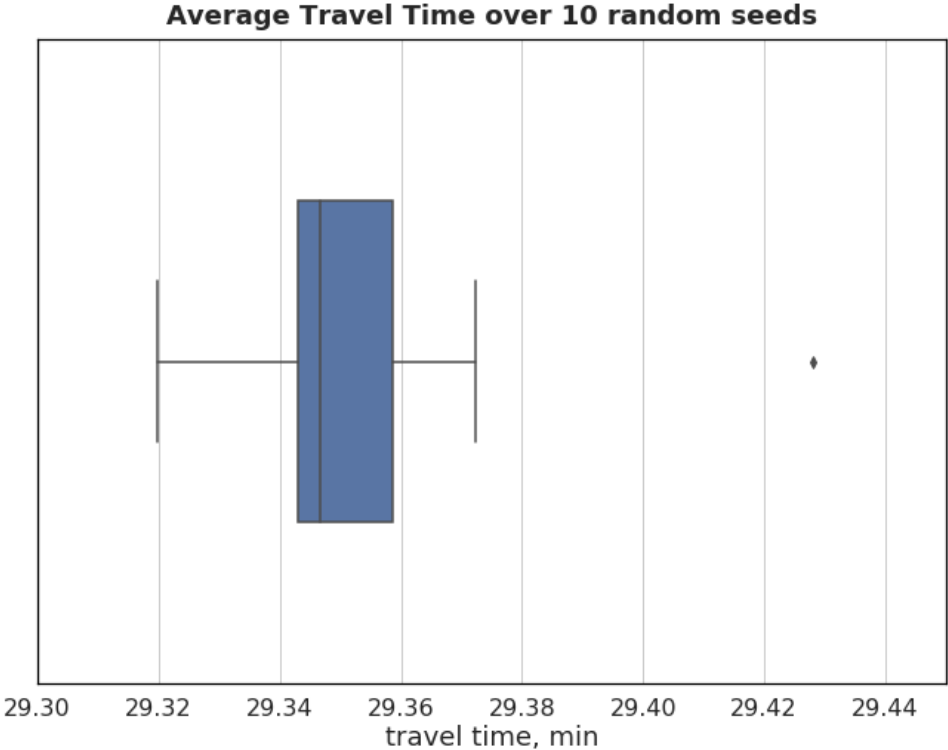
Figure 5.1   Travel time variation over 10 runs.
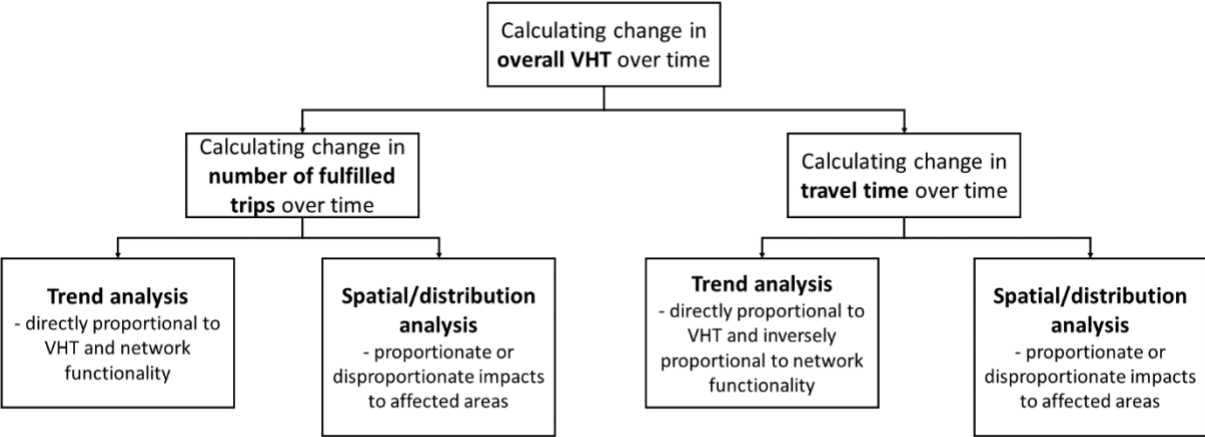
Figure 5.2   Assessing impacts to transportation networks.
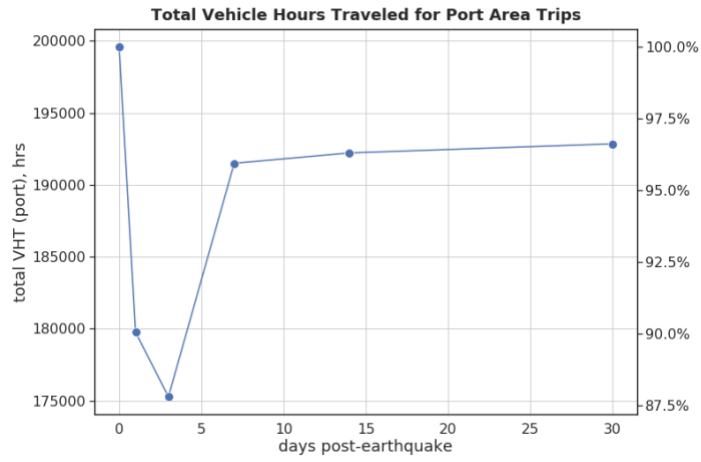
(a) Change in total VHT
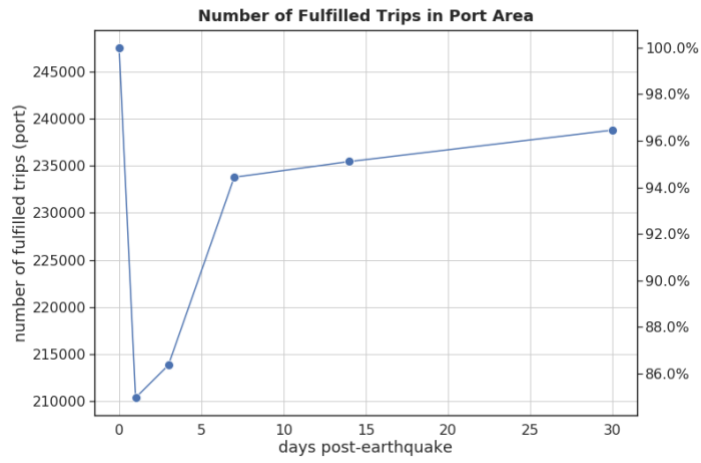
(b) Change in fulfilled trips
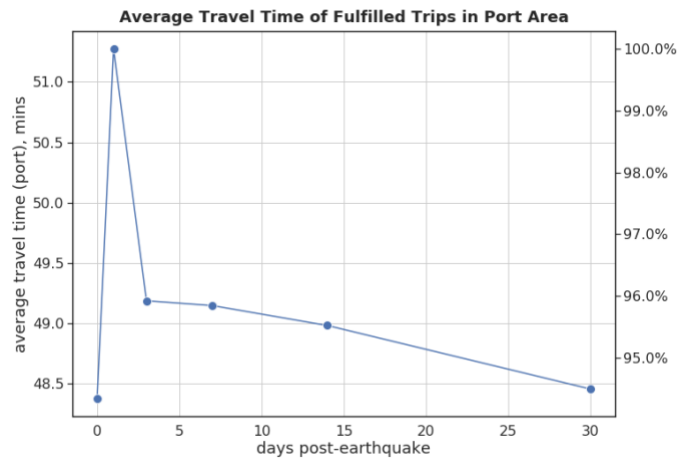
(c) Change in average travel time

Figure 5.3   Simulation results.
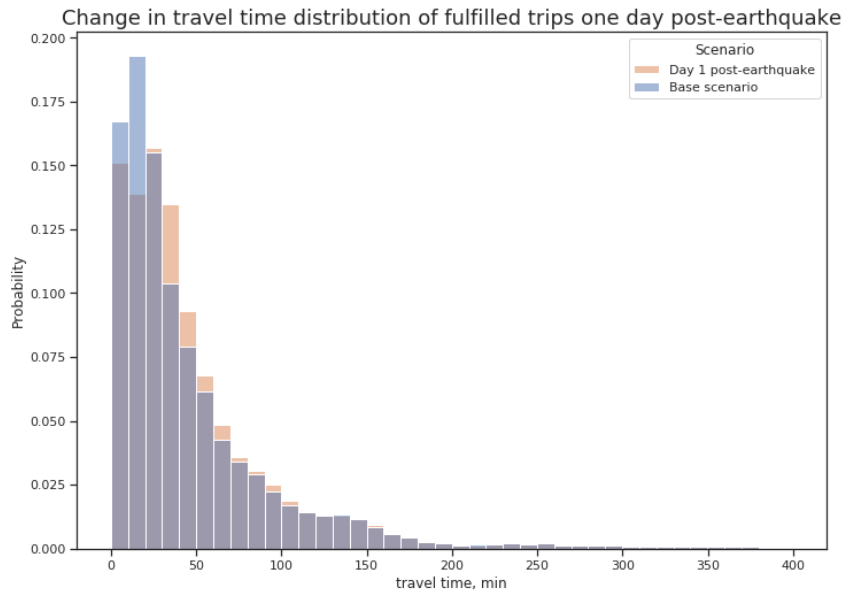
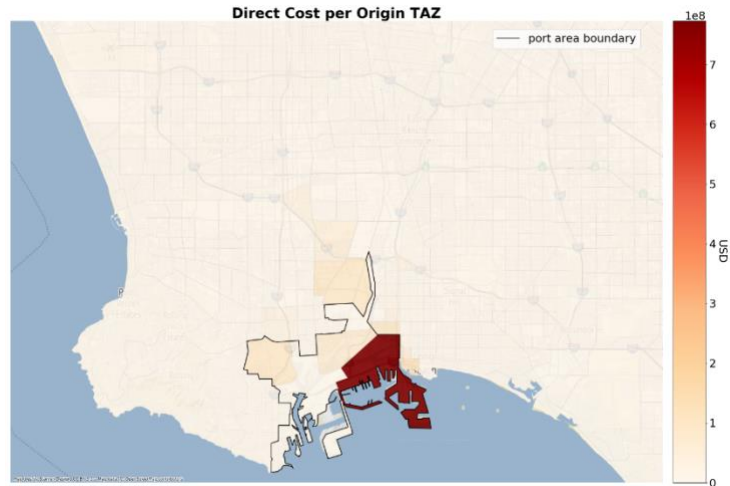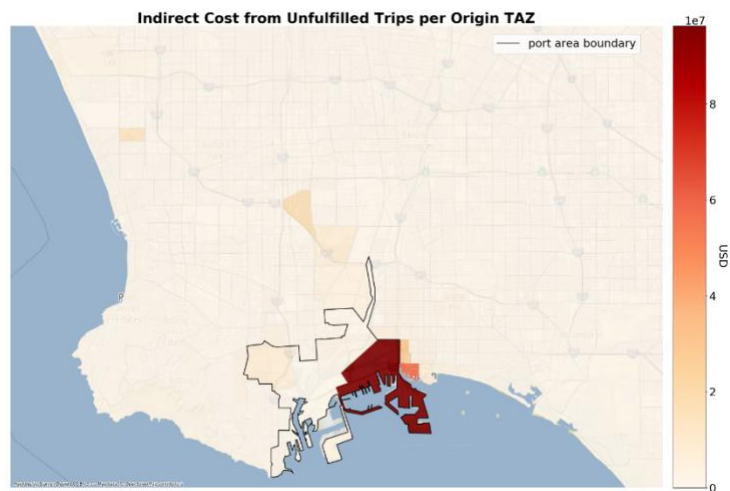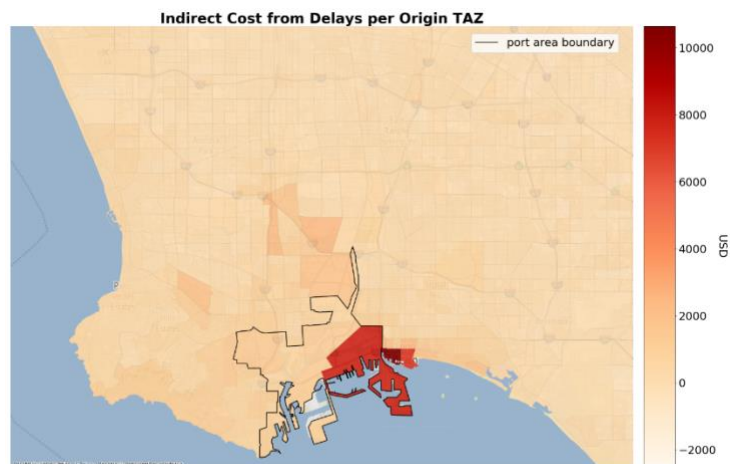**Figure 5.4   Travel time distribution of port area trips.**
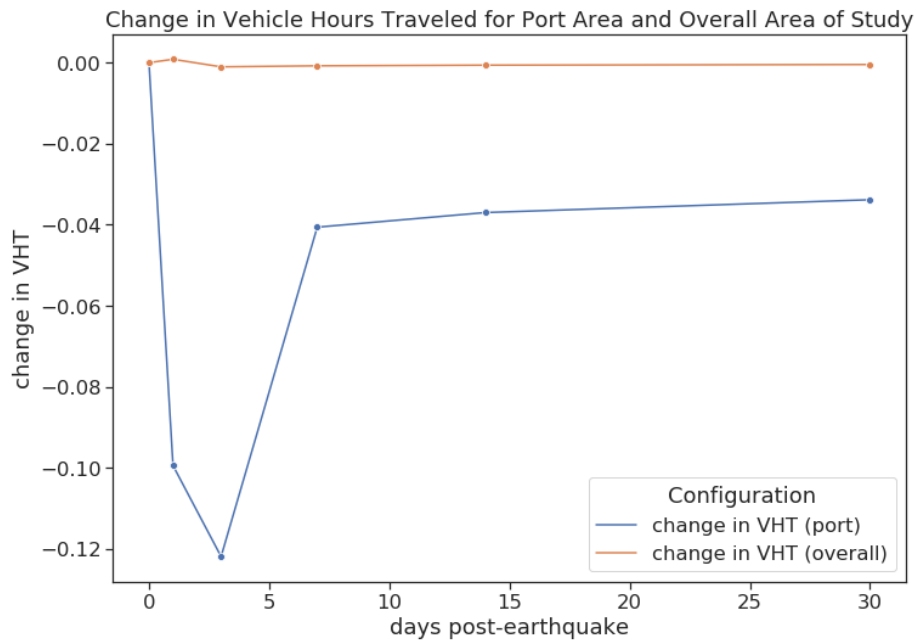
Figure 5.5   Change in VHT (overall area vs. port area).
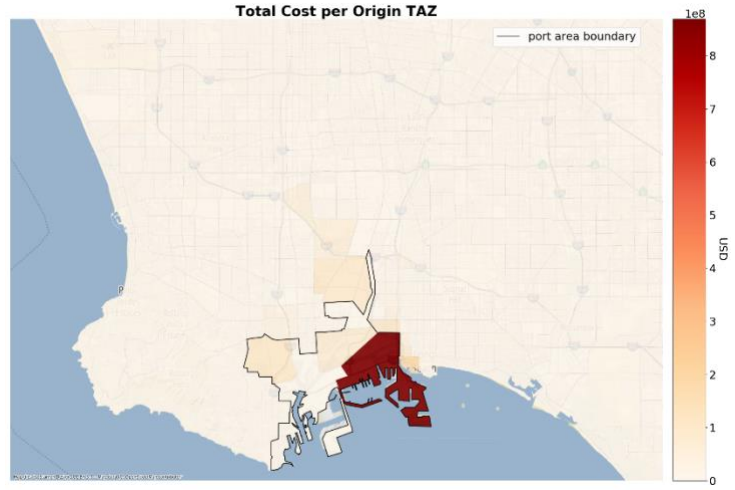
(a) Direct cost

(b) Indirect cost from unfulfilled trips

(c) Indirect cost from delays

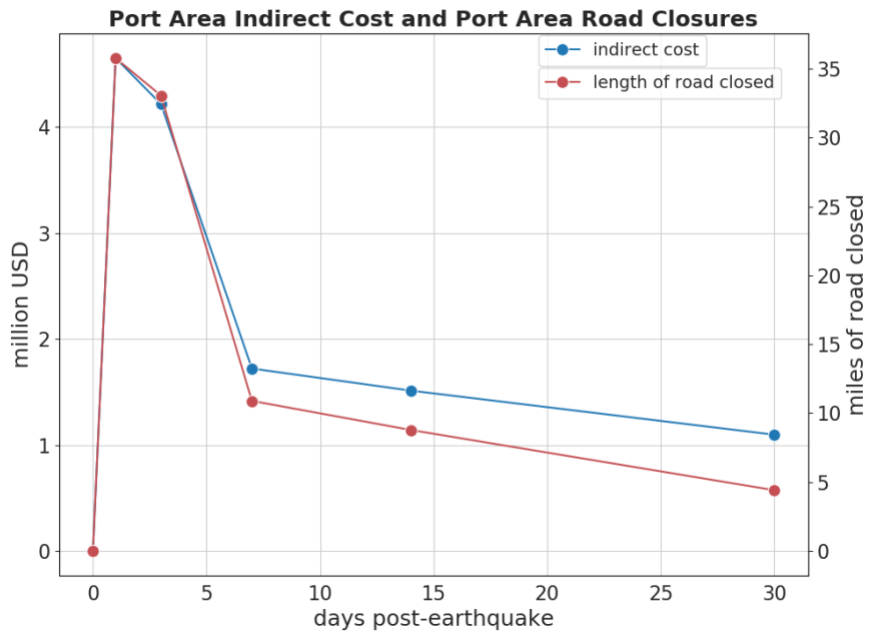(d) Total cost

Figure 5.6   Cost per origin TAZ.
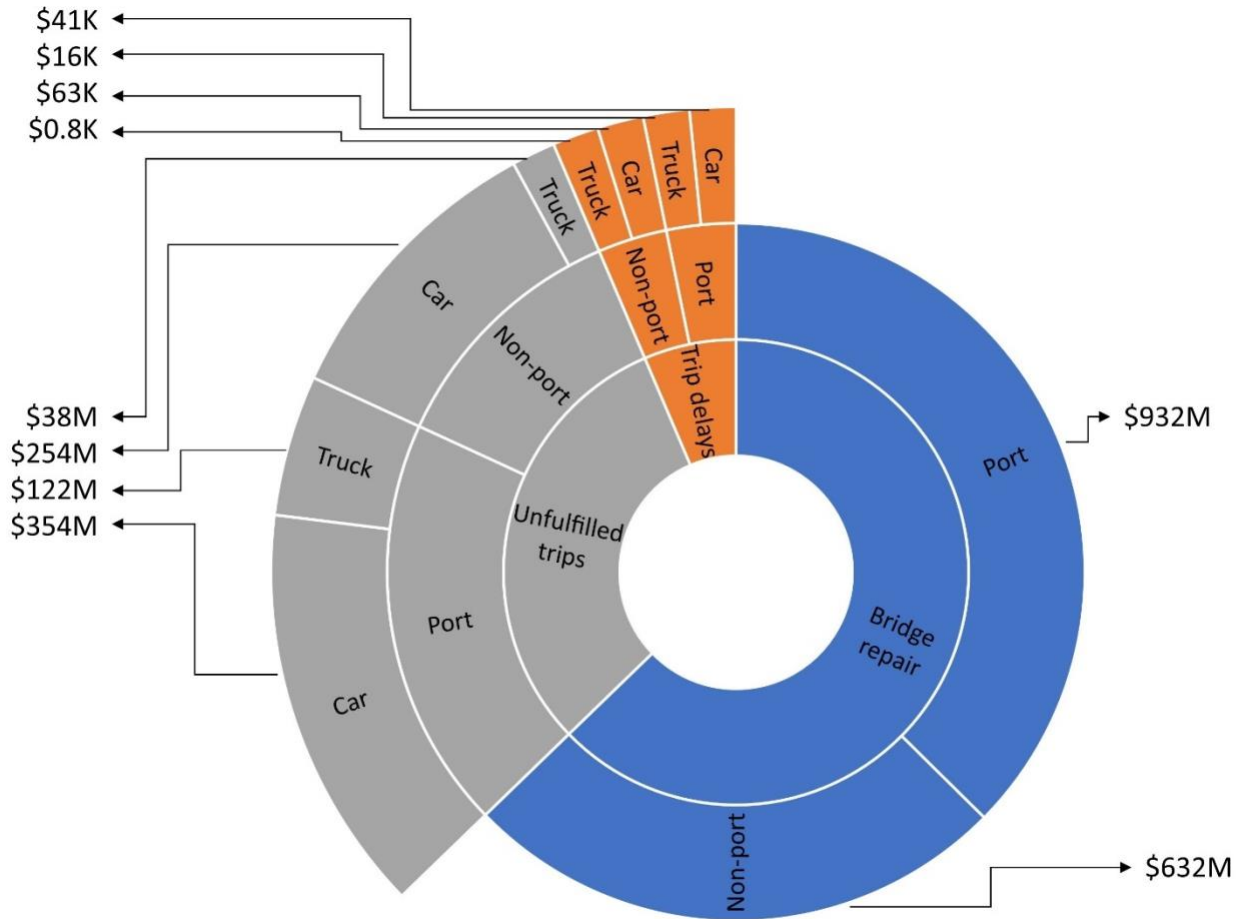

Figure 5.7   Indirect cost and road closures.

Figure 5.8   Cost estimate visualization.

41

6   SUMMARY, CONCLUSIONS, AND SUGGESTED FUTURE WORK

This report presented a highly granular synthesis framework to quantify the resilience of transportation networks to hazards such as earthquakes, including seismic loss and recovery. The framework starts with the characterization of the hazard and determining the probable seismic demands. The second step is the assessment of damage to the bridge infrastructure, which is carried out by individually modeling the bridges and simulating their responses in order to obtain individual bridge-level seismic fragility curves. These seismic fragility curves can then be used to rapidly estimate damage under hypothetical scenarios (which is the approach taken here) or real-life events. The resulting estimated damage (i.e., functionality losses) are then used as inputs to a transportation network analysis, which runs an agent-based semi-dynamic traffic assignment on the network over a 24-hour period under the base scenario pre-earthquake and the modified networks post-earthquake. The output road usage and individual agent travel times are then used for estimating the economic impact of the earthquake on the transportation network through direct costs (repair) and indirect costs (delays, loss of connectivity). The resolution offered by this framework on a regional level allows for a holistic and detailed assessment of seismic impacts to transportation systems.

The case study on two neighboring Southern California ports (Los Angeles and Long Beach) produced results on predicted bridge damage and closures, delays, and road network disconnections for a hypothetical Magnitude 7.4 earthquake for a network with 1,444,790 edges and 615,174 nodes and 8,404,218 agents, a scale not commonly seen in research of this nature. The simulation results were verified to have similar values compared to real-life travel time and travel distance metrics. The granularity of results allowed for trend analysis and a deeper spatial analysis of commonly aggregated metrics like vehicle hours traveled (VHT) in the system and of each agent. Furthermore, an economic impact estimation indicated that the port area, which is closest to the epicenter of the earthquake, is disproportionately affected, with the overall losses consisting largely of direct losses (repairing or replacing the damaged bridges) followed by lost demand. Losses due to congestion/delay were found to be minimal as traffic was still able to flow in and out of the ports (albeit at a significantly diminished level initially) and because not all of the connecting bridges would collapse or otherwise lose their functionality.

To improve this resilience assessment and recovery prediction framework, considering different modes of transport and having more information on a vehicles' activity (e.g., work, leisure, etc.) or more information on freight payload and its corresponding value can help in better quantifying the economic cost of each trip and the overall economic impact to the transportation network. One important outcome of the transportation-centric loss analysis used in this study is the ability to compare it with current budget allocations for disaster prevention, such as seismic retrofitting and

bridge repairs, and understanding the impact of delaying these tasks, which in the case study led to a 50% increase in indirect costs to individuals on top of repair costs.

REFERENCES

Alipour, A., Shafei, B., 2016. Seismic resilience of transportation networks with deteriorating components. Journal of Structural Engineering 142, C4015015.

American Road and Transportation Builders Association, 2022. California 2022 bridge profile. https://artbabridgereport.org/reports/state/CA.pdf. Accessed: 2022-11-16.

ASCE, 2021. 2021 Report Card for America's Infrastructure. Technical Report. American Society of Civil Engineers (ASCE).

Baker, J., Bradley, B., Stafford, P., 2021. Seismic Hazard and Risk Analysis. Cambridge University Press. doi:10.1017/9781108425056.

Baker, J.W., Lin, T., Shahi, S.K., Jayaram, N., 2011. New ground motion selection procedures and selected motions for the PEER transportation research program. Technical Report. Pacific Earthquake Engineering Research Center.

Berdica, K., 2002. An introduction to road vulnerability: what has been done, is done and should be done. Transport policy 9, 117–127.

Bhattacharjee, G., Baker, J.W., 2021. Using global variance-based sensitivity analysis to prioritise bridge retrofits in a regional road network subject to seismic hazard. Structure and Infrastructure Engineering , 1–14.

Boeing, G., 2017. Osmnx: New methods for acquiring, constructing, analyzing, and visualizing complex street networks. Computers, Environment and Urban Systems 65, 126–139.

Brookshire, D.S., Chang, S.E., Cochrane, H., Olson, R.A., Rose, A., Steenson, J., 1997. Direct and indirect economic losses from earthquake damage. Earthquake Spectra 13, 683–701.

Caltrans, 2019. Caltrans Seismic Design Criteria Version 2.0. State of California Department of Transportation.

Cetiner, B., 2020. Image-Based Modeling of Bridges and Its Applications to Evaluating Resiliency of Transportation Networks. Ph.D. thesis. University of California, Los Angeles. Los Angeles, CA.

Chan, C., Kuncheria, A., Zhao, B., Cabannes, T., Keimer, A., Wang, B., Bayen, A., Macfarlane, J., 2021. Quasi-dynamic traffic assignment using high performance computing URL: https://arxiv.org/abs/2104.12911, doi:10.48550/ARXIV.2104.12911.

Chang, L., Elnashai, A.S., Spencer Jr, B.F., 2012. Post-earthquake modelling of transportation networks. Structure and infrastructure Engineering 8, 893–911.

Chang, S.E., Nojima, N., 2001. Measuring post-disaster transportation system performance: the 1995 kobe earthquake in comparative perspective. Transportation research part A: policy and practice 35, 475–494.

Chen, L., Zhu, Y., Papandreou, G., Schroff, F., Adam, H., 2018. Encoder-decoder with atrous separable convolution for semantic image segmentation. CoRR abs/1802.02611. URL: http://arxiv.org/abs/1802.02611,arXiv:1802.02611.

Cho, S., Gordon, P., Moore II, J.E., Richardson, H.W., Shinozuka, M., Chang, S., 2001. Integrating transportation network and regional economic models to estimate the costs of a large urban earthquake. Journal of Regional Science 41, 39–65.

Colak, S., Lima, A., Gonzalez, M.C., 2016. Understanding congested travel in urban areas. Nature communications 7, 10793.

Cooper, J.D., Friedland, I.M., Buckle, I.G., Nimis, R., McMullin, B.N., 1994. The northridge earthquake: Progress made, lessons learned in seismic-resistant bridge design. Public roads 58, 26–36. URL: http://www.fhwa.dot.gov/publications/publicroads/94summer/p94su26.cfm.

Dong, Y., Frangopol, D.M., Saydam, D., 2014. Sustainability of highway bridge networks under seismic hazard. Journal of earthquake engineering 18, 41–66.

Elwood, K.J., 2004. Modelling failures in existing reinforced concrete columns. Canadian Journal of Civil Engineering 31, 846–859. URL: https://doi.org/10.1139/l04-040, doi:10.1139/l04-040.

Federal Highway Administration, 1995. Recording and coding guide for the structure inventory and appraisal of the nation's bridges. Technical Report Report No. FHWA-PD-96-001. US Department of Transportation.

FEMA, 2003. Hazus-MH 2.1 Technical Manual: Earthquake Model. Federal Emergency Management Agency. Washington, DC.

Feng, K., Li, Q., Ellingwood, B.R., 2020. Post-earthquake modelling of transportation networks using an agent-based model. Structure and Infrastructure Engineering 16, 1578–1592.

FHWA, 1995. Recording and Coding Guide for the Structure Inventory and Appraisal of the Nation's Bridges. Technical Report. Report No. FHWAPD-96-001, US Department of Transportation, Federal Highway Administration, Office of Engineering Bridge Division, Washington, DC.

Foti, F., Waddell, P., Luxen, D., 2012. A generalized computational framework for accessibility: from the pedestrian to the metropolitan scale, in: Proceedings of the 4th TRB Conference on Innovations in Travel Modeling. Transportation Research Board.

Frangopol, D.M., Bocchini, P., 2011. Resilience as optimization criterion for the rehabilitation of bridges belonging to a transportation network subject to earthquake, in: Structures Congress 2011, pp. 2044–2055.

Goldberg, M.A., 1975. On the inefficiency of being efficient. Environment and Planning A 7, 921–939.

Gordon, P., Moore II, J.E., Richardson, H.W., Shinozuka, M., An, D., Cho, S., 2004. Earthquake Disaster Mitigation for Urban Transportation Systems: An Integrated Methodology that Builds on the Kobe and Northridge Experiences. Modeling Spatial and Economic Impacts of Disasters , 205–232doi:10.1007/978-3-540-24787-6{_}11.

Ham, H., Kim, T.J., Boyce, D., 2005. Assessment of economic impacts from unexpected events with an interregional commodity flow and multimodal transportation network model. Transportation Research Part A: Policy and Practice 39, 849–860.

Jaiswal, K., Bausch, D., Rozelle, J., Holub, J., McGowan, S., 2017. Hazus® estimated annualized earthquake losses for the United States. Technical Report FEMA P-366. Federal Emergency Management Agency.

Jalayer, F., Cornell, C.A., 2009. Alternative non-linear demand estimation methods for probability-based seismic assessments. Earthquake Engineering & Structural Dynamics 38, 951–972. URL: https://onlinelibrary.wiley.com/doi/abs/10.1002/eqe.876, doi:https://doi.org/10.1002/eqe.876.

Kawashima, K., Buckle, I., 2013. Structural performance of bridges in the tohoku-oki earthquake. Earthquake Spectra 29, 315–338. URL: https://doi.org/10.1193/1.4000129, doi:10.1193/1.4000129.

Khademi, N., Balaei, B., Shahri, M., Mirzaei, M., Sarrafi, B., Zahabiun, M., Mohaymany, A.S., 2015. Transportation network vulnerability analysis for the case of a catastrophic earthquake. International journal of disaster risk reduction 12, 234–254.

Khalili-Tehrani, P., Shamsabadi, A., Stewart, J.P., Taciroglu, E., 2016. Backbone curves with physical parameters for passive lateral response of homogeneous abutment backfills. Bulletin of Earthquake Engineering 14, 3003–3023. doi:10.1007/s10518-016-9934-3.

Koc, E., Cetiner, B., Rose, A., Soibelman, L., Taciroglu, E., Wei, D., 2020. Craft: Comprehensive resilience assessment framework for transportation systems in urban areas. Advanced Engineering Informatics 46, 101159. URL: https://www.sciencedirect.com/science/article/pii/S1474034620301300, doi:https://doi.org/10.1016/j.aei.2020.101159.

Leontief, W., 1986. Input-output economics. Oxford University Press.

Mangalathu, S., 2017. Performance based grouping and fragility analysis of box-girder bridges in California. Ph.D. thesis. Georgia Institute of Technology. Atlanta, GA.

Mattsson, L.G., Jenelius, E., 2015. Vulnerability and resilience of transport systems–a discussion of recent research. Transportation Research Part A: Policy and Practice 81, 16–34.

McGuire, R.K., 2001. Deterministic vs. probabilistic earthquake hazards and risks. Soil Dynamics and Earthquake Engineering 21, 377–384.

McKenna, F., 2011. Opensees: A framework for earthquake engineering simulation. Computing in Science & Engineering 13, 58–66. doi:10.1109/MCSE.2011.66.

Modarres, M., Zarei, B., 2002. Application of network theory and ahp in urban transportation to minimize earthquake damages. Journal of the Operational Research Society 53, 1308–1316.

Moehle, J., Deierlein, G.G., 2004a. A framework methodology for performance-based earthquake engineering, in: Proceedings of the 13th World Conference on Earthquake Engineering, pp. 3812–3814. doi:10.1061/9780784412121.173.

Moehle, J., Deierlein, G.G., 2004b. A framework methodology for performance-based earthquake engineering, in: 13th world conference on earthquake engineering.

Muthukumar, S., 2003. A Contact Element Approach with Hysteresis Damping for the Analysis and Design of Pounding in Bridges. Ph.D. thesis. Georgia Institute of Technology.

Nakanishi, H., Matsuo, K., Black, J., 2013. Transportation planning methodologies for post-disaster recovery in regional communities: the east japan earthquake and tsunami 2011. Journal of Transport Geography 31, 181–191.

Neuenhofer, A., Filippou, F.C., 1997. Evaluation of Nonlinear Frame Finite-Element Models. Journal of Structural Engineering 123, 958–966. doi:10.1061/(asce)0733-9445(1997)123:7(958).

Nielson, B.G., 2005. Analytical fragility curves for highway bridges in moderate seismic zones. Georgia Institute of Technology.

Nikoo, N., Babaei, M., Mohaymany, A.S., 2018. Emergency transportation network design problem: Identification and evaluation of disaster response routes. International journal of disaster risk reduction 27, 7–20.

Nojima, N., Sugito, M., 2000. Simulation and evaluation of post-earthquake functional performance of transportation network, in: Proceedings of the 12th world conference on earthquake engineering, New Zealand Society for Earthquake Engineering Upper Hutt.

Pabilonia, S., Jadoo, M., Khandrika, B., Price, J., Mildenberger, J., 2019. BLS publishes experimental state-level labor productivity measures. Monthly Labor Review URL: https://doi.org/10.21916/mlr.2019.12,doi:10.21916/mlr.2019.12.

Padgett, J.E., DesRoches, R., Nilsson, E., 2010. Regional seismic risk assessment of bridge network in charleston, south carolina. Journal of Earthquake Engineering 14, 918–933.

Payne, H.J., 1979. Freflo: A macroscopic simulation model of freeway traffic. Transportation Research Record .

Ramanathan, K., Padgett, J.E., DesRoches, R., 2015. Temporal evolution of seismic fragility curves for concrete box-girder bridges in California. Engineering Structures 97, 29–46. URL: https://www.sciencedirect.com/science/article/pii/S0141029615002229,doi:10.1016/J.ENGSTRUCT.2015.03.069.

Shafieezadeh, A., Ramanathan, K., Padgett, J.E., DesRoches, R., 2012. Fractional order intensity measures for probabilistic seismic demand modeling applied to highway bridges. Earthquake Engineering & Structural Dynamics 41, 391–409. URL: https://onlinelibrary.wiley.com/doi/abs/10.1002/eqe.1135, doi:https://doi.org/10.1002/eqe.1135.

Silva, P.F., Megally, S., Seible, F., 2009. Seismic Performance of Sacrificial Exterior Shear Keys in Bridge Abutments. Earthquake Spectra 25, 643–664. URL: http://journals.sagepub.com/doi/10.1193/1.3155405,doi:10.1193/1.3155405.

Small, P., Gill, D., Maechling, P.J., Taborda, R., Callaghan, S., Jordan, T.H., Olsen, K.B., Ely, G.P., Goulet, C., 2017. The SCEC Unified Community Velocity Model Software Framework. Seismological Research Letters 88, 1539–1552. URL: https://doi.org/10.1785/0220170082, doi:10.1785/0220170082,arXiv:https://pubs.geoscienceworld.org/ssa/srl/article-pdf/88/6/1539/3950255/srl/article-pdf/88/6/1539/3950255/srl-2017082.1.pdf.

Southern California Association of Governments, 2020. Connect SoCal – The 2020-2045 Regional Transportation Plan/Sustainable Communities Strategy. Technical Report. Southern California Association of Governments.

Suarez, P., Anderson, W., Mahal, V., Lakshmanan, T., 2005. Impacts of flooding and climate change on urban transportation: A systemwide performance assessment of the boston metro area. Transportation Research Part D: transport and environment 10, 231–244.

Tatano, H., Tsuchiya, S., 2008. A framework for economic loss estimation due to seismic transportation network disruption: a spatial computable general equilibrium approach. Natural Hazards 44, 253–265.

USBPR, 1964. United States Bureau of Public Roads Traffic Assignment Manual for Application with a Large, High-speed Computer. volume 2.

Vasconcelos, F., Barreto, J.P., Boyer, E., 2018. Automatic camera calibration using multiple sets of pairwise correspondences. IEEE Transactions on Pattern Analysis and Machine Intelligence 40, 791–803. doi:10.1109/TPAMI.2017.2699648.

Wu, Y., Hou, G., Chen, S., 2021. Post-earthquake resilience assessment and long-term restoration prioritization of transportation network. Reliability Engineering & System Safety 211, 107612.

Zhao, B., Kumar, K., Casey, G., Soga, K., 2019. Agent-Based Model (ABM) for City-Scale Traffic Simulation: A Case Study on San Francisco. ICE Publishing. pp. 203–212. URL: https://www.icevirtuallibrary.com/doi/abs/10.1680/icsic.64669.203,doi:10.1680/icsic.64669.203, arXiv:https://www.icevirtuallibrary.com/doi/pdf/10.1680/icsic.64669.203.

Zhou, Y., Banerjee, S., Shinozuka, M., 2010. Socio-economic effect of seismic retrofit of bridges for highway transportation networks: a pilot study. Structure and Infrastructure Engineering 6, 145–157.

Zhou, Y., Qi, H., Ma, Y., 2019. End-to-end wireframe parsing, in: ICCV 2019.

PEER Core Institutions

University of California, Berkeley (Lead Institution)
California Institute of Technology
Oregon State University
Stanford University
University of California, Davis
University of California, Irvine
University of California, Los Angeles
University of California, San Diego
University of Nevada, Reno
University of Southern California
University of Washington